IEEE Robotics and Automation Letters (RAL) paper presented at the
2020 IEEE/RSJ International Conference on Intelligent Robots and Systems (IROS)
October 25-29, 2020, Las Vegas, NV, USA (Virtual)

Energy Management Through Footstep Selection For Bipedal Robots*

Steven Crews and Matthew Travers

***Abstract*— This work proposes a method of footstep placement that controls system energy to enable a dynamically-safe walking behavior. Contrasting many other works that treat rough terrain as a series of disturbances that need to be mitigated with control, we provide some insight into how energy-targeted foot placement is enough to allow a passive system to transit over rough terrain. This work explores the underlying complexities of one of the simplest walking models, the inverted pendulum, which, in its various forms, is the skeleton behind all bipedal robots, from Asimo to Atlas. Troubling all of these humanoids is the foot placement problem, especially when the terrain is not flat. This work uses analysis of the system energy to divide the feasible stepping area into regions that would either enable dynamic walking or cause a fall. Second we subdivide the walking region into sectors that promote the accumulation or dissipation of energy, stimulating or inhibiting future steps. Third, we introduce a method of global energy management using a moving reference point over rough terrain. We present results on how these concepts can be used to prevent falls, accumulate energy to cross gaps, and even enable a passive system to walk uphill.**

I. Introduction

Consider a child racing down the side of a hill, running and jumping with little cognitive thought and attention into the mechanics of running, yet motion is natural, dynamic and graceful. The child quickly grasps that long steps slow or stop her while short steps speed her up. Intrinsically, the child adjusts step length to maintain a constant, comfortable speed. Using foot placement to control energy and change speeds is a foundation for dynamic legged motion and the central idea of this work.

Our core contribution is a method that uses foot contacts to steer the body center of mass (COM) along energy profiles over rough terrain. We use a simplified model to illustrate how leg placement affects system energy and movement. This work derives two boundaries that are fundamental to walking: the first separates walking from falling while the second subdivides walking into slowing down and speeding up. We develop strategies for accumulating energy prior to gap crossing and walking uphill.

It is the authors' understanding that the following contributions are new to dynamic walking over rough terrain. We demonstrate how energy-centric foot placement can permit a passive system to move over rough terrain, rather than rejecting terrain through feedback. Through an analysis of the post-impact energy, we show that the reachable foothold positions can be divided into regions that permit walking or cause falling per Fig. 1. Step placement is not simply determining whether the system will fall or not, but also where it can step to ensure future steps have enough energy to succeed. We then subdivide the walking region into sectors that either assist, maintain, or hinder walking. It will be shown that knowledge of these sectors are imperative to the accumulation or dissipation of energy, even if the terrain map is not perfect. Finally, we generate a strategy of tracking a moving global reference point, enabling a passive robot to follow a constant energy profile across rough terrain in the same way it would as if the ground were flat.

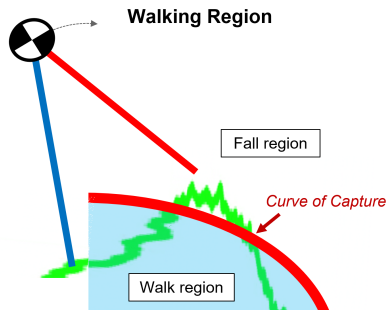

Fig. 1. The space of kinematically-feasible footstep regions can be divided by the *curve of capture* into regions that either promote dynamic walking or falling backwards.

The paper is structured as follows. Sect. II describes related works. We separate the kinematically-feasible step region into areas of dynamic relavance using a *curve of capture* and *curve of equal energy*, defined in Sections III-A and III-B. In Sect. III-C, we present a method for maintaining *equivalent energy* to some moving global reference. We present results for these methods using a passive nonlinear inverted pendulum (NIP) model walking over very rough terrain in Sect. IV. Our Conclusions and proposed future work are in Sections V and VI. In the Appendix, we include additional regression details and a link to the code for duplicability of results.

II. Background

One of the greatest strides in biped walking came forth in the early 1990s when McGeer introduced the passive kneed walker [1], [2], a system of two interacting pendula using gravity as a means of compelling forward motion. The system balanced energy through an interplay of ground contacts (kinetic energy [KE] lost) and traveling down a slope (potential energy [PE] gained), starting a trend of passive walking analysis [3]–[10]. By interacting with the ground by passive dynamics alone, this system was robust to minor disturbances, asymptotically stable around a limit cycle. Although using a relatively simple yet elegant model, the body of works most importantly demonstrated that walk-

*This work was not supported by any organization

Biorobotics Lab, Robotics Institute, Carnegie Mellon University, 5000 Forbes Ave, USA (screws, mtravers) @andrew.cmu.edu

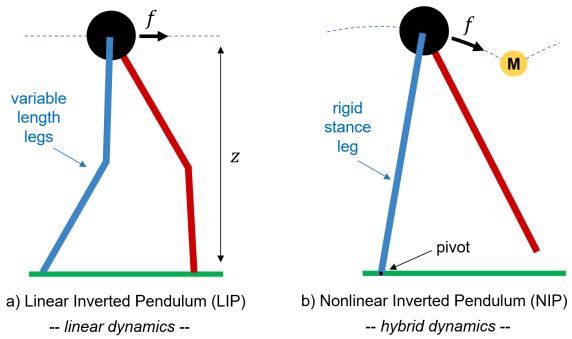

Fig. 2. Simple Walking Models with Massless Legs. a) LIP legs provide the vertical force ($F = mg$) necessary to maintain the COM at a constant height z, smoothly moving through elastic contact with the ground.b) The rigid NIP system pivots about the stance foot, moving the COM along an arc with nonlinear dynamics f. At swing foot contact, the system loses energy through a discontinuous, inelastic collision M.

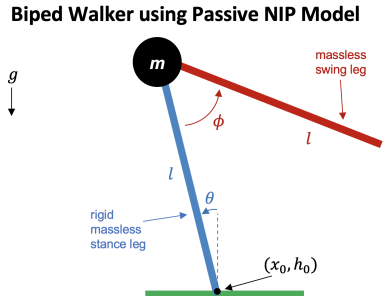

Fig. 3. Passive NIP Biped. Point mass at the hip, with pin joint at stance foot. Massless swing leg can be arbitrarily placed without dynamic implications.

ing does not always require control. In a similar way, this work takes a step back to the passive NIP model walking down a hill.

A. System Model

The simplest approximation of a walking system is a point mass with massless legs, of which there are two basic variants: the LIP and the NIP, shown in Fig. 2. The linear inverted pendulum (LIP) model consists of a point mass at the hip with variable-length legs that have enough control authority to maintain the COM at a constant height z [11], [12], Although this model seems overwhelmingly simple, the LIP model is heavily used for footstep planning and trajectory control [13]–[20]. Key LIP assumptions are that step impact is smooth and continuous, creating no discrete events. The LIP model is powerful since it allows the system to be approximated completely using linear dynamics.

The NIP model handles walking motion instead with a stiff stance leg with its COM traveling along an arc of length l. The stiff leg creates an arcing motion at the hip that is much more human-like than walking with constant height hips. Although more lifelike, this bio-mimetic motion complicates the dynamics such that they are no longer linear and no longer restricted to the horizontal plane. Additionally, the continuous dynamics are interrupted by the swing leg impacting the ground, creating hybrid dynamics. Similar to [12], [21]–[26], the following assumptions are made:

1) The body consists of a point mass, modeled at the hip. The legs are massless.
2) At impact, there is an instantaneous transfer of support from the old stance leg to the new stance leg (old swing leg). Only one leg is in contact with the ground at a time (no double support phase).
3) Ground impact is inelastic and the system does not rebound/bounce upon impact.
4) The stance foot does not slip and acts as an uncontrolled pin joint (some of the referenced papers use friction models and/or ankle control).

B. Continuous Dynamics

The single support, or swing phase, of the legged NIP is given by the Lagrangian $\mathcal{L}$

$$\mathcal{L} = \mathcal{T} - \mathcal{U} \tag{1}$$

$$\mathcal{T} = \frac{ml^2}{2}\dot{\theta}^2 \qquad \mathcal{U} = mgl\cos\theta, \tag{2}$$

where $\mathcal{T}$ and $\mathcal{U}$ are the system KE and PE, l is the length from the stance foot pivot to mass m, and Angle θ is the rotation of the pendulum per Fig. 3. The dynamic equations derived from (1) are shown to be

$$\frac{d}{dt}\left(\frac{\partial \mathcal{L}}{\partial \dot{\theta}}\right) - \frac{\partial \mathcal{L}}{\partial \theta} = 0 \tag{3}$$

$$ml^2\ddot{\theta} = mgl\sin\theta \tag{4}$$

For state space $\mathbf{x} = \begin{bmatrix}\theta & \dot{\theta}\end{bmatrix}^{\mathrm{T}}$, the NIP double integrator can be rewritten as

$$\dot{\mathbf{x}} = \begin{bmatrix}\dot{\theta} \\ \frac{g}{l}\sin\theta\end{bmatrix} \tag{5}$$

C. Impact Dynamics

The swing leg impacts the ground with a rigid and non-conservative impact, wherein kinetic energy (KE) is lost from the system and an instantaneous change in pivot point occurs. Although energy is lost into the ground at foot contact, momentum is conserved about the foot touchdown point and thus the momentum about the swing toe before impact L^- is equal to the angular momentum about the stance foot after impact L^+, where the nomenclature $^-,^+$ is used to describe information immediately before or after collision.

The angular momentum L for a system can be given by

$$\mathbf{L} = m\mathbf{r}_{\mathrm{com}} \times (\boldsymbol{\omega} \times \mathbf{r}_{\mathrm{o}}) \tag{6}$$

Where $\mathbf{r}_{\mathrm{com}} = \begin{bmatrix}-l\sin(\theta) & l\cos(\theta) & 0\end{bmatrix}$ is the vector from point of rotation to the COM, $\mathbf{r}_{\mathrm{o}}$ is the vector from the touchdown point to the COM, and $\boldsymbol{\omega} = \begin{bmatrix}0 & 0 & \dot{\theta}\end{bmatrix}^T$ is the rotation rate vector. Applying (6) to the system shown in Fig. 4, the pre- and post-collision angular momentum can be given by

$$\begin{aligned}\mathbf{L}^- =& m\begin{bmatrix}-l\sin\theta \\ l\cos\theta \\ 0\end{bmatrix}^- \times \left(\begin{bmatrix}0 \\ 0 \\ \dot{\theta}\end{bmatrix}^- \times \begin{bmatrix}l\sin(\theta+\phi) \\ l\cos(\theta+\phi) \\ 0\end{bmatrix}^-\right) \\ =& \begin{bmatrix}0 & 0 & ml^2\cos(\phi^-)\dot{\theta}^-\end{bmatrix}^T\end{aligned} \tag{7}$$

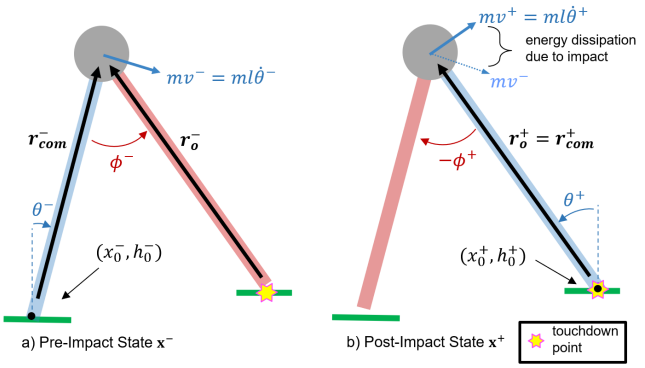

Fig. 4. Angular Momentum About Impact Foot showing Pre- and Post-Impact Configurations. (a) Pre-Impact State $\mathbf{x}^-$. (b) Post-Impact State $\mathbf{x}^+$.

$$\begin{aligned}\mathbf{L}^+ =& m \begin{bmatrix} -l\sin\theta \\ l\cos\theta \\ 0 \end{bmatrix}^+ \times \left(\begin{bmatrix} 0 \\ 0 \\ \dot{\theta} \end{bmatrix}^+ \times \begin{bmatrix} -l\sin\theta \\ l\cos\theta \\ 0 \end{bmatrix}^+ \right) \\ =& \begin{bmatrix} 0 & 0 & ml^2\dot{\theta}^+ \end{bmatrix}^T \end{aligned} \tag{8}$$

By equating (7) and (8), we can relate the velocity before impact $\dot{\theta}^-$ to the velocity after impact $\dot{\theta}^+$. Additionally, through the kinematics seen in Fig. 4, we can relate the pre- and post-collision configurations, ($\theta^+ = \theta^- + \phi^-$) and ($\phi^+ = -\phi^-$). Together, these kinematic and momentum relationships form the discrete impact map function M

$$\begin{aligned}\mathbf{x}^+ &= M(\mathbf{x}^-) \\ \begin{bmatrix} \theta \\ \phi \\ \dot{\theta} \end{bmatrix}^+ &= \begin{bmatrix} 1 & 1 & 0 \\ 0 & -1 & 0 \\ 0 & 0 & \cos\phi^- \end{bmatrix} \begin{bmatrix} \theta \\ \phi \\ \dot{\theta} \end{bmatrix}^- .\end{aligned} \tag{9}$$

It is important to note that since the swing leg is considered massless and can be placed arbitrarily, the inter-leg angle ϕ does not appear in the continuous dynamics (5) but does appear in the discrete impact map (9).

D. Capture Point

Based on the dynamics of a LIP, *capture point* (CP) [12] was developed as a means of controlling a force disturbance. A CP is a terrain location that the robot can step in order to come to a complete stop. Although the idea of CP can apply to all forms of dynamic walking, researchers have used the concept primarily around the simplified dynamics model of the LIP during zero moment point (ZMP) [27] walking. ZMP walking maintains the ZMP within the support polygon, but allows the floor projected COM to deviate during a gait. For a known COM trajectory, the CP is very fast to calculate and therefore very useful in push recovery [12], [28]–[34], i.e. step on CP to cease movement.

We borrow the CP concept from these ZMP LIP bipeds and extend it to a NIP biped for a different purpose. Rather than using CP to cease motion on the NIP, this work uses CP as a stability metric to ensure motion is occurring at each step. Given a CP over some terrain gradient, it can be quickly computed whether the current step size will result in forward motion, stopping, or falling backwards, as shown in Fig. 5. This paper will show that many CPs exist along a curve herein known as the *curve of capture*. By monitoring this curve for each step, this paper will demonstrate online step sequence generation over uneven terrains.

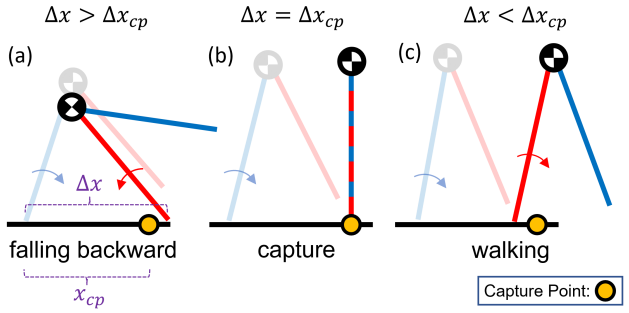

Fig. 5. Stepping Relative to Capture Point x_{cp}. (a) Overstepping the CP results in falling backwards. (b) Stepping directly onto a CP results in the NIP stopping at the unstable equilibrium point. (c) Stepping before the CP results in a walking behavior.

III. Technical Approach

A. Curve of Capture

Pratt [12] introduced the idea of capture point (CP) to the LIP model. The core use was foot placement as a means of push recovery. Other works extended the idea of CP to the NIP [25], [35] as a target for foot placement to cease motion. This work uses the idea of CP as a boundary for successful walking over uneven terrain. Instead of just a theoretical means of stopping motion, the CP can be defined as a boundary between walking and falling backwards as shown in Fig. 5.

Computing the NIP CP is relatively straight forward, but there is no analytical solution. It begins with an understanding that capture occurs when the post-collision energy is equal to the max PE of the system ($E^+ = \mathcal{U}_{max}$) when the NIP is stationary and vertical (see Fig. 5). The local change between foot origin horizontal position Δx and height Δh in the global frame (x_o, h_o) (see Fig. 4) is described by

$$\begin{aligned}\Delta x &= x_o^+ - x_o^- = l\sin(\theta^- + \phi^-) - l\sin\theta^- \\ \Delta h &= h_o^+ - h_o^- = l\cos\theta^- - l\cos(\theta^- + \phi^-)\end{aligned} \tag{10}$$

This section assumes that E refers to the local energy of a step (Sect. III-C introduces the concept of energy relative to some other reference point). Assuming we know the pre-impact energy of a step E^-, we need to determine foot placement to dissipate all of the KE at the unstable equilibrium point $\mathcal{T} = \dot{\theta}^+ = 0$ and $E^+ = \mathcal{U}$. Using (5), we can determine the post-collision energy relationship in terms of pre-collision components

$$\begin{aligned}\Delta E &= (\mathcal{T}^+ + \mathcal{U}^+) - (\mathcal{T}^- + \mathcal{U}^-) \\ mgl - E^- &= -\frac{ml^2}{2}\left(\dot{\theta}^-\right)^2 \sin^2\theta^- \\ &\quad + mgl\left(\cos(\theta^- + \phi^-) - \cos\theta^-\right).\end{aligned} \tag{11}$$

Since the system is passive, we can compute the impact velocity

$$\dot{\theta}^- = -\sqrt{\frac{2}{ml^2}\left(E^- - mgl\cos\theta^-\right)}. \tag{12}$$

Substituting (12) into (11) yields an expression that is dependent only upon pre-collision configuration

$$\begin{aligned} mgl - E^- = &-\left(E^- - mgl\cos\theta^-\right)\sin^2\theta^- \\ &+ mgl\left(\cos\left(\theta^- + \phi^-\right) - \cos\theta^-\right). \end{aligned} \tag{13}$$

By substituting (10) into (13)

$$mgl\left(1 + mgl\Delta h\right) - E^- = \left(mgl\cos\theta^- - E^-\right)\sin^2\theta^-, \tag{14}$$

it becomes clear that there is a matching leg position for a given toe height Δh, assuming only walking configurations ($-\frac{\pi}{2} < \theta^- < \frac{\pi}{2}$ and $E^- > E^+$). Since (14) does not have a closed-form solution, this work uses a least-square polynomial regression of sampled points in the space to determine the relationship between energy and configuration that reaches the CP, whose coefficients are shown in the Appendix

$$\Delta x_{cp} = R_{cp}\left(E^-, \Delta h\right). \tag{15}$$

The shape of the regression R_{cp} is shown in Fig. 6. As energy increases, the biped can step higher and further prior to reaching the CP.

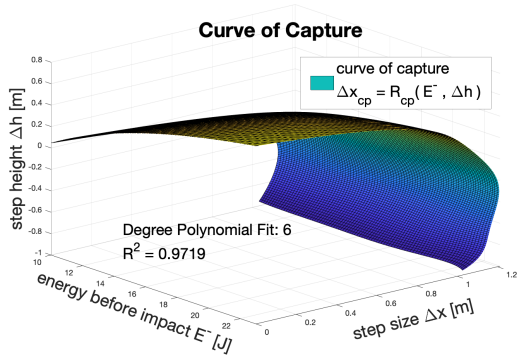

Fig. 6. *Curve of Capture*

This curve provides a very intuitive meaning: everything to the left of the curve results in a walking behavior and everything to the right results in falling backwards as seen if Fig. 7. As a robot is walking and looking for a safe place to step that ensures forward motion, this curve creates the boundary for dynamically-safe walking behavior.

B. *Curve of Equal Energy*

Another important step location for a system is the location where local energy is conserved. Consider a biped walking down a slope. The system gains PE by walking down the slope, but loses KE at impact. Short steps result in a quick-stepping behavior that increases energy ($E^+ > E^-$). Stepping too far, but not yet to the CP, results in the system

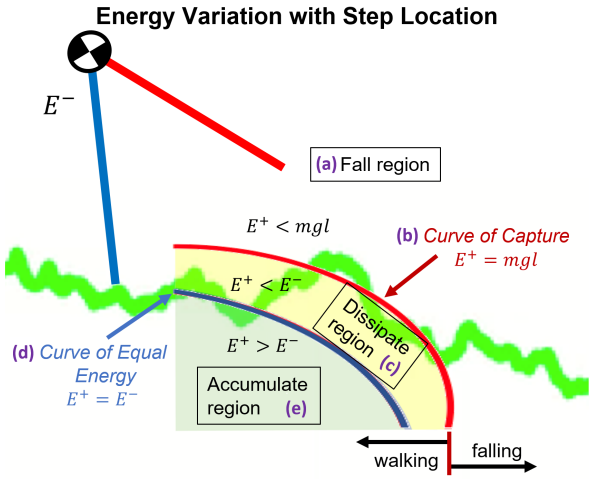

Fig. 7. Energy Variation with Step Location. (a) Stepping on terrain beyond the *curve of capture* means the system does not have the energy to reach the vertical position and results in falling backwards. (b) Stepping onto the *curve of capture* is the exact energy required to stop at the unstable equilibrium point. Stepping below this curve results in walking. (c) Stepping into the dissipate region results in walking, but a loss in energy. (d) Stepping directly onto the *curve of equal energy* means the KE lost through impact is equal to the PE gained. (e) Stepping into the accumulate region results in speeding up, where subsequent steps have more local energy than the previous step.

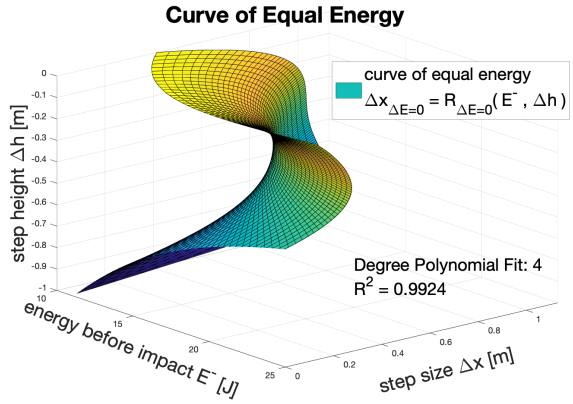

Fig. 8. *Curve of Equal Energy*

losing energy ($E^+ < E^-$), but still takes a step. There is a specific step length that corresponds to a steady-state gait ($v_{n+1} = v_n$) or ($E^+ = E^-$) (equivalent to a fixed point on a return map). By setting $\Delta E = 0$ for the NIP, we arrive at the expression

$$mgl\Delta h = \left(mgl\cos\theta^- - E^-\right)\sin^2\theta^-. \tag{16}$$

Similar to (14), this work uses a least-square polynomial regression to determine the relationship between energy and configuration that reaches the equal energy, whose coefficients are shown in the Appendix

$$\Delta x_{\Delta E=0} = R_{\Delta E=0}\left(E^-, \Delta h\right). \tag{17}$$

The shape of the regression $R_{\Delta E=0}$ is shown in Fig. 8.

This curve denotes an important concept: step to the left to speed up or to the right to slow down. Although qualitative,

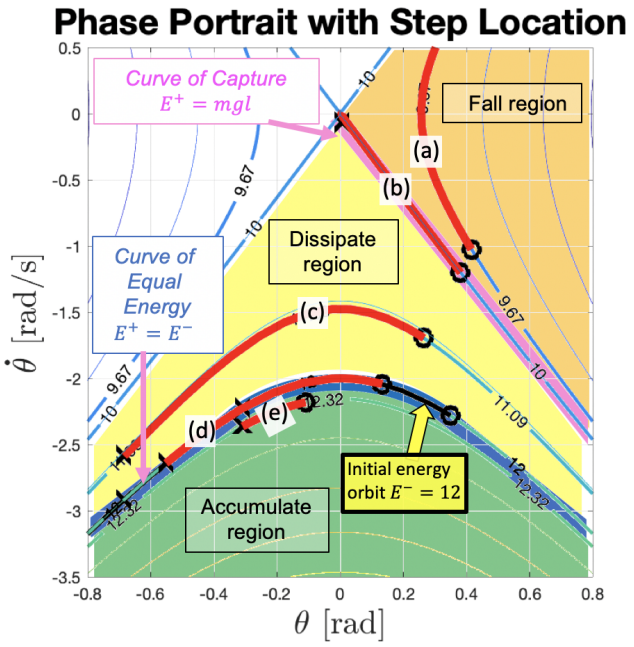

Fig. 9. Phase Portrait with Step Location. These red paths represent what happens when stepping into the regions shown in Fig. 7 with $mgl = 10$. Contours represent energy levels. (a) Overstepping the *curve of capture* results in oscillation (falling backwards). (b) Stepping onto the *curve of capture* takes the system up the homoclinic orbit to the separatrix. (c) Losing energy with a long step, but still walking. (d) Stepping onto *curve of equal energy* returns to same rotation orbit. (e) Gaining energy with a short step.

not quantitative in nature, this curve helps inform us where to step to increase or decrease system energy. If the robot must speed up to overcome an approaching obstacle, it can accumulate energy by taking several steps to the left of the curve. Likewise, if moving too fast, step to the right of the curve to dissipate energy.

The regions separated by the *curve of capture* and *curve of equal energy* can be depicted by the phase portrait [36] of a simple pendulum (see Fig. 9). Stepping directly onto the *curve of equal energy* results in maintaining the same energy level as the traveling orbit. Stepping short/long result in energy increase/decrease. Stepping on the *curve of capture* puts the system directly onto the homoclinic orbit which takes it to the unstable equilibrium point (separatrix). Stepping past the *curve of capture* results in an pendulum-like behavior (walker falling backwards).

C. Equivalent Energy

The final idea to develop is the idea of *equivalent energy*. Consider the same passive NIP walking down a hill, but this time over uneven terrain with an uphill section (see Fig. 10). Ensuring individual step placement is below the *curve of capture* or in vicinity of the *curve of equal energy* does not guarantee that the biped will be able to make it over the hump. This is because the previous two curves are local energy curves and we require an additional strategy of tracking the global energy required to overcome the global PE at the hump. It is already known that if the robot walks along the constant slope from origin to the hump by stepping

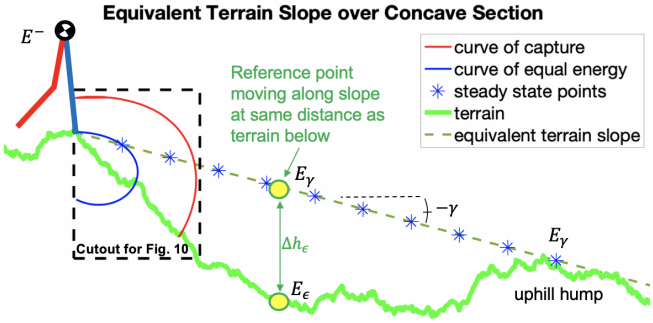

Fig. 10. Equivalent Terrain Slope over Concave Section. By following the *curve of equal energy*, the biped can walk down the slope $-\gamma$ that connects the current position and the future uphill hump. The robot increases KE as it travels along the terrain under the slope to maintain the energy equivalent to walking along the artificial terrain slope.

along the *curve of equal energy* it will reach the hump with the original system energy E^-. We use this as a basis to derive a strategy that ensures the system maintains the energy equivalent to walking down this slope at steady state velocity. At points below the curve, the system must speed up (add KE to make up for lost PE), and slow down above the curve.

The target energy at any point Δx varies with Δh along the equivalent terrain slope γ. Therefore as the biped steps some distance Δx, it must expect a global loss of PE that must be stored in the form of KE

$$\begin{aligned} -\Delta\mathcal{U}_\gamma &= -mg\Delta h_\gamma \\ &= -mg\Delta x \tan\gamma = \Delta\mathcal{T}_\epsilon, \end{aligned} \tag{18}$$

where $\Delta\mathcal{U}_\gamma$ is the expected PE loss due to the change in slope γ and $\Delta\mathcal{T}_\epsilon$ is the equivalent increase in KE. Similar to the equal energy approach, the goal is to balance the total energy. Though, instead of local energies E^- and E^+, we must refer to the equivalent terrain slope as a reference. This allows us to know whether we are above or below the target energy required to traverse the hump. In order to compute the equivalent PE at impact, the equivalent height Δh_ϵ^+ must be computed

$$\Delta h_\epsilon^+ = \Delta h_\epsilon^- + \Delta h - \Delta h_\gamma. \tag{19}$$

To illustrate this idea, consider the change in height relative to the target slope (see Fig. 11). If the next foothold location is closer to the equivalent terrain slope than the previous step ($\Delta h < \Delta h_\gamma$ results in $\Delta h_\epsilon^+ < \Delta h_\epsilon^-$), then the system will be able to lose KE and maintain the same *equivalent energy* ($E_\epsilon^+ = E_\epsilon^-$). Using (19), the post-collision *equivalent energy* E_ϵ^+ can be computed relative to the equivalent terrain slope

$$E_\epsilon^+ = mg\left(\Delta h_\epsilon^- + \Delta h - \Delta x \tan\gamma\right) + \tfrac{m}{2}\left(l\cos\theta^-\dot{\theta}^-\right)^2. \tag{20}$$

In order to make use of *equivalent energy*, it is necessary to not only identify the configuration(s) where our post-collision equivalent energy is equal to the desired energy along the slope ($E_\epsilon^+ = E_\gamma$), but also it is important to know the foothold positions in which E_ϵ^+ increases or decreases

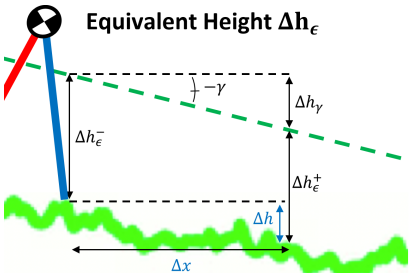

Fig. 11. Equivalent Height Δh_ϵ shows the height relative to the target slope. This is essential in computing the equivalent PE.

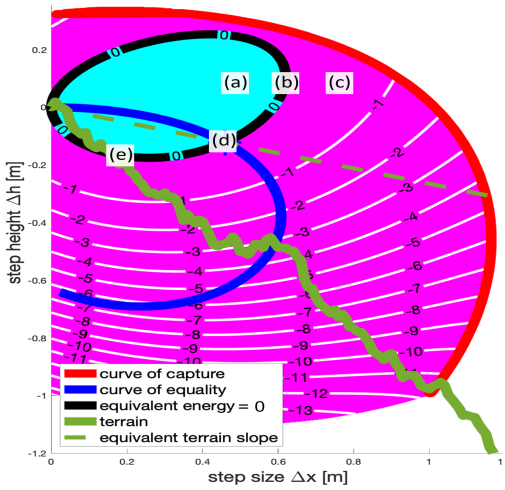

Fig. 12. Equivalent Energy (cutout from Fig. 10) represents the energy equivalent to walking down the terrain slope relative to a desired energy level E_γ. The contours equate to the difference $E_\epsilon^+ - E_\gamma$. (a) The blue region has higher energy ($E_\epsilon^+ > E_\gamma$). (b) Stepping along this equivalent energy curve results in the same energy as required along the curve ($E_\epsilon^+ = E_\gamma$) or ($\Delta KE + \Delta PE = 0$). Stepping from this curve results in achieving E_γ as if stepping directly onto the equivalent terrain slope. (c) By stepping into the pink region, the robot loses more energy than required to transit the equivalent terrain slope ($E_\epsilon^+ < E_\gamma$). (d) The *curve of equal energy* and the equivalent terrain slope intersection defines the energy baseline for this figure. (e) Desired stepping point for this terrain, in which energy is equivalent to walking along the equivalent terrain slope at steady state velocity.

relative to E_γ. For a single step, the difference $E_\epsilon^+ - E_\gamma$ is represented in the contours of Fig. 12. This plot shows the curve in which the equivalent energy is less than, equal to, or greater than the energy required on the slope. Stepping anywhere along the black curve equates to stepping along the slope at (d). The system will gain or lose E_ϵ^+ by stepping in the blue or pink regions, respectively. While it this method can be done with only a one-step terrain horizon, the steps can be better sequenced using a horizon of the entire terrain map. Underlying this curve is an exchange of local KE and PE that will be shown in Section IV.

IV. Results

A. Using the Curve of Equal Energy and Curve of Capture to Cross a Gap

This first test consists of accumulating energy to cross a gap in the terrain (see Fig. 13). Initially, the reference gap *curve of capture* is well below the lip of the far side of the

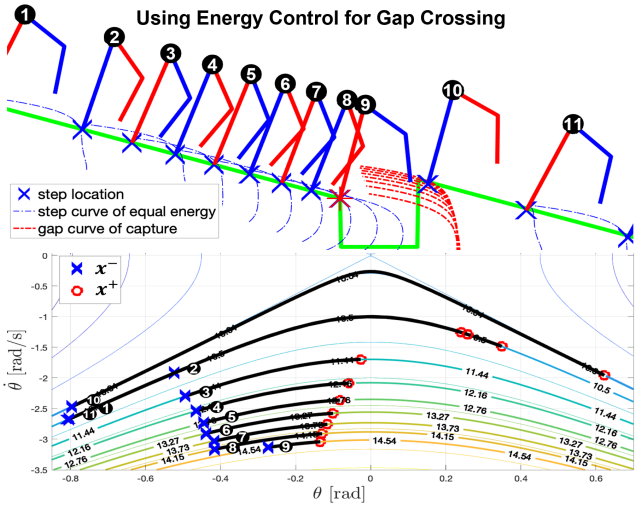

Fig. 13. Using Energy Control for Gap Crossing. $E_{min} = mgl = 10J$. For step (1), the robot starts with energy = $10.5J$ at steady state. During steps (2)-(8), the robot steps to the left of the *curve of equality* to accumulate energy. As the robot accumulates energy, the *curve of capture* across the gap incrementally pushes up. At step (9), the biped has just enough energy to cross the gap ($E^+ = 10.05J$). For steps (10)-(11), the biped returns to step locations that result in the nominal walking energy.

gap. For 7 steps, the robot places its foot to the left of the *curve of equal energy*, adding local energy to the system. At each step, the gap *curve of capture* expands, pushing upward. By step 9, the gap *curve of capture* pushed over the far side of the gap, ensuring the system could safely step. Depicted by the transition from $\mathbf{x}_9^-$ to $\mathbf{x}_{10}^+$ in the corresponding phase portrait, the system lost $4.5J$ of energy crossing the gap, indicating that the capture point energy was approximately $14.5J$. The system did not have enough energy to cross the gap in the first 8 steps. This demonstration assumes that the gap position and height is known in advance. If the gap came sooner, then the system would have to step further to the left of the *curve of equal energy* to accumulate energy quicker. Link to video.

B. Crossing a Valley with Equivalent Energy

For this final test, we use the metric of *equivalent energy* to assist the passive robot on an uphill section. As shown in Fig. 14, the robot sets a target location on the horizon and draws an equivalent terrain slope. The strategy here is simple: as long as the biped can maintain its total *equivalent energy* at or above the desired energy level of this slope, it will be able to summit the uphill section. We start the robot at $v_o = 1m/s$, or $E^- = 10.5J$, barely enough energy to passively walk down the slope. In order to maintain its *equivalent energy*, the biped must add KE to account for the lost PE (relative to the equivalent terrain slope above the terrain). In order to keep walking, the energy in local coordinates must always be above the max PE of the system $E > 10J$.

This result shows the trade-off between KE and PE. As noted in Section III-C, the equivalent energy curve only keeps the robot walking at *exactly* the equivalent energy

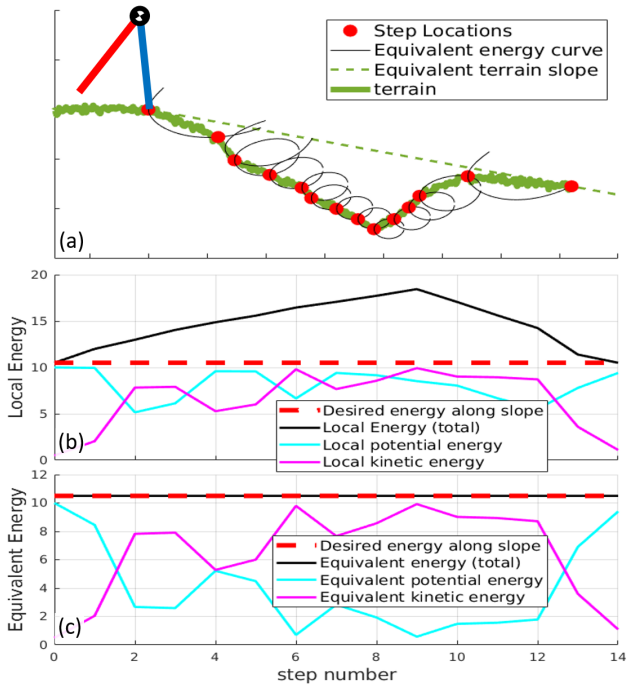

Fig. 14. Managing Equivalent Energy. Robot starts with barely enough energy to maintain forward motion $E = 10.5J$. ($m = l = 1$,$g = 10$) (a) Passive biped walking down a slope, then up another. The biped uses foothold placement along equivalent energy curves to ensure the desired energy ($10.5J$) along the equivalent terrain slope is maintained. (b) System energy, with PE measured locally from foothold position. (c) System energy, with PE measured from equivalent terrain slope. Robot maintains total equivalent energy at $10.5J$ throughout. Notice symmetry of PE/KE curves. As the robot loses PE, the robot must add KE to make up for it.

of the slope. In this experiment, the robot strategy was to step directly onto the curve, but it could have used far more aggressive strategies to maximize energy. If the robot were to step into the interior of any of the curves, the *equivalent energy* would have increased above $10.5J$, giving the system additional energy to accomplish more challenging terrains. It is important to note that this KE/PE tradeoff also works above the equivalent terrain slope. If the terrain is higher than the slope, the biped must lose KE to balance the gained PE, but be very careful to always step behind the curve of capture to ensure it has enough energy to continue walking.

V. Conclusion

This work proposed a method of footstep placement that controls system energy to enable a dynamically-safe walking behavior. We separated the kinematically-feasible foothold locations into regions defined by energy levels. Based on the notion of capture point, we constructed the *curve of capture* that divides the walking and falling regions for a NIP biped. We developed a *curve of equal energy* that further separates the walking region into areas that either increase or decrease the level of energy. By tracking the energy of a global moving reference, we unfolded the *equivalent energy*, a technique that allows passive systems to overcome uphill sections in rough terrains through proper foot placement in the preceding steps. Knowledge of these regions empower energy-based foothold positioning that steers the body COM.

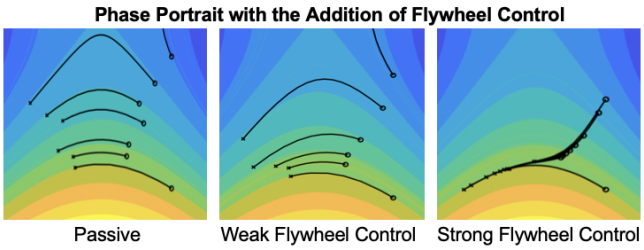

Fig. 15. The flywheel helps return the system to an energy orbit during the swing phase of an orbit.

We demonstrated that a passive NIP-inspired centroidal biped can walk robustly over uneven terrain by using only footstep placement under various scenarios.

VI. Future Work

This work can be extended to 3D walking, wherein the robot must be able to maintain its footsteps behind the *curve of capture* in the sagittal plane while simultaneously over the *curve of capture* in the frontal plane. This would ensure forward motion while maintaining stability through oscillating back and forth between left and right feet.

Although these energy regions were only demonstrated on a passive system traveling downhill, the concepts apply directly to actively-controlled systems as well. By adding an energy-stabilization technique such as swinging a leg mass, bending a torso, or spinning a flywheel, the fairly small regions identified in this work can be significantly expanded. For example, by adding a simple flywheel as per [12], [25], [37], [38] and a simple energy-based control algorithm, the energy level can be stabilized as seen in Fig. 15. It was beyond the scope of this paper to include active stabilization and foothold positioning, it is imperative to mention that these ideas work well together. Finally, we are building a robot to demonstrate the ideas covered within this work.

Appendix

This section contains the regression data to reconstruct the *curve of capture* and *curve of equal energy*. The regression data below matches the results from Figures 6 and 8. The input regression data is normalized by its mean μ and standard deviation σ as follows.

$$E_*^- = \frac{E^- - \mu_E}{\sigma_E} \qquad \Delta h_*^- = \frac{\Delta h^- - \mu_{\Delta h}}{\sigma_{\Delta h}}, \tag{21}$$

where E_*^- and Δh_* represent the normalized input data. The respective mean and standard deviation data are located in Tables I and II. The normalized data can be taken to their respective power and multiplied by the coefficients of regression from the tables.

$$\Delta x = \sum_{m=0}^{O} \sum_{n=0}^{O} c_{m,n} \left(E_*^-\right)^m \left(\Delta h_*\right)^n \tag{22}$$

Where O represents the order of the system as listed in Section III. Using (22) and information from Tables I and II, the Δx footstep positions for (15) and (17) can be recreated very quickly. The regression code is available at this link.

TABLE I

COEFFICIENTS FOR *Curve of Capture* POLYNOMIAL

power coefficient n of the step height $(\Delta h_*)^n$	$m=0$	$m=1$	$m=2$	$m=3$	$m=4$	$m=5$	$m=6$
6	-0.0002						
5	0.0271	0.0220					
4	-0.1503	-0.1926	-0.0432				
3	0.2642	0.5905	0.3149	0.0419			
2	-0.1146	-0.6912	-0.7842	-0.2731	-0.0284		
1	-0.0080	0.1626	0.6898	0.5426	0.1466	0.0129	
0	1.0236	-0.0883	-0.1225	-0.2628	-0.1736	-0.0449	-0.0042

	E^-	Δh
μ	14.5588	0.0283
σ	4.0225	0.2898

power coefficient m of the scaled pre-collision energy $(E_*^-)^m$

TABLE II

COEFFICIENTS FOR *Curve of Equal Energy* POLYNOMIAL

power coefficient n of the step height $(\Delta h_*)^n$	$m=0$	$m=1$	$m=2$	$m=3$	$m=4$
4	0.0133				
3	-0.0935	0.0001			
2	0.2021	0.0401	-0.0390		
1	-0.2750	0.0563	-0.0198	0.0498	
0	0.4126	-0.0507	-0.0681	-0.0018	-0.0088

	E^-	Δh
μ	18.2337	-0.2576
σ	8.0842	0.1616

power coefficient m of the scaled pre-collision energy $(E_*^-)^m$

REFERENCES

[1] T. McGeer, "Stability and control of two-dimensional biped walking," *Center for Systems Science, Simon Fraser University, Burnaby, BC, Canada, Technical Report*, vol. 1, 1988.

[2] T. McGeer, "Passive Dynamic Walking," *Int. Journal Robotics Research*, vol. 9, no. 2, pp. 62–82, 1990.

[3] A. Goswami, B. Espiau, and A. Keramane, "Limit cycles in a passive compass gait biped and passivity-mimicking control laws," *Autonomous Robots*, vol. 4, no. 3, pp. 273–286, 1997.

[4] B. Thuilot, A. Goswami, and B. Espiau, "Bifurcation and chaos in a simple passive bipedal gait," in *International Conference on Robotics and Automation*, vol. 1. IEEE, 1997, pp. 792–798.

[5] M. W. Spong, "Passivity based control of the compass gait biped," *IFAC Proceedings Volumes*, vol. 32, no. 2, pp. 506–510, 1999.

[6] A. D. Kuo, "Stabilization of lateral motion in passive dynamic walking," *The International journal of robotics research*, vol. 18, no. 9, pp. 917–930, 1999.

[7] K. Osuka and K.-I. Kirihara, "Motion analysis and experiment of passive walking robot Quartet II," *Journal of the Robotics Society of Japan*, vol. 18, no. 5, pp. 737–742, 2000.

[8] M. W. Spong and G. Bhatia, "Further results on control of the compass gait biped," in *International Conference on Intelligent Robots and Systems*, vol. 2. IEEE, 2003, pp. 1933–1938.

[9] F. Asano, "Stability analysis of passive compass gait using linearized model," in *2011 IEEE International Conference on Robotics and Automation*. IEEE, 2011, pp. 557–562.

[10] H. Gritli, N. Khraief, and S. Belghith, "Falling of a passive compass-gait biped robot caused by a boundary crisis," in *Chaotic Modeling and Simulation International Conference, Greece*, 2011, pp. 155–162.

[11] S. Kajita, F. Kanehiro, K. Kaneko, K. Yokoi, and H. Hirukawa, "The 3D Linear Inverted Pendulum Mode: A simple modeling for a biped walking pattern generation," in *International Conference on Intelligent Robots and Systems*, vol. 1. IEEE, 2001, pp. 239–246.

[12] J. Pratt, J. Carff, S. Drakunov, and A. Goswami, "Capture point: A step toward humanoid push recovery," in *2006 6th IEEE-RAS international conference on humanoid robots*. IEEE, 2006, pp. 200–207.

[13] S. Kajita, F. Kanehiro, K. Kaneko, K. Fujiwara, K. Harada, K. Yokoi, and H. Hirukawa, "Resolved momentum control: Humanoid motion planning based on the linear and angular momentum," in *International Conference on Intelligent Robots and Systems*, vol. 2. IEEE, 2003, pp. 1644–1650.

[14] J. Chestnutt, M. Lau, G. Cheung, J. Kuffner, J. Hodgins, and T. Kanade, "Footstep planning for the honda asimo humanoid," in *International conference on robotics and automation*. IEEE, 2005, pp. 629–634.

[15] I.-W. Park, J.-Y. Kim, J. Lee, and J.-H. Oh, "Online free walking trajectory generation for biped humanoid robot KHR-3 (HUBO)," in *International Conference on Robotics and Automation*. IEEE, 2006, pp. 1231–1236.

[16] J. Englsberger, C. Ott, M. A. Roa, A. Albu-Schäffer, and G. Hirzinger, "Bipedal walking control based on capture point dynamics," in *International Conference on Intelligent Robots and Systems*. IEEE, 2011, pp. 4420–4427.

[17] F. Ferro and L. Marchionni, "Reem: A humanoid service robot," in *First Iberian Robotics Conference*. Springer, 2014, pp. 521–525.

[18] J. Englsberger, A. Werner, C. Ott, B. Henze, M. A. Roa, G. Garofalo, R. Burger, A. Beyer, O. Eiberger, K. Schmid, *et al.*, "Overview of the torque-controlled humanoid robot TORO," in *International Conference on Humanoid Robots*. IEEE, 2014, pp. 916–923.

[19] O. Stasse, T. Flayols, R. Budhiraja, K. Giraud-Esclasse, J. Carpentier, J. Mirabel, A. Del Prete, P. Souères, N. Mansard, F. Lamiraux, *et al.*, "TALOS: A new humanoid research platform targeted for industrial applications," in *International Conference on Humanoid Robotics*. IEEE, 2017, pp. 689–695.

[20] A. W. Winkler, F. Farshidian, D. Pardo, M. Neunert, and J. Buchli, "Fast trajectory optimization for legged robots using vertex-based zmp constraints," *IEEE Robotics and Automation Letters*, vol. 2, no. 4, pp. 2201–2208, 2017.

[21] M. W. Spong and F. Bullo, "Controlled symmetries and passive walking," in *IFAC Proceedings*, vol. 35, 2002, pp. 557–562.

[22] R. Tedrake, "Underactuated Robotics: Learning, Planning, and Control for Efficient and Agile Machines: Course Notes for MIT 6.832," *MIT OpenCourseware*, 2009.

[23] I. Manchester and J. Umenberger, "Real-time planning with primitives for dynamic walking over uneven terrain," in *International Conference on Robotics and Automation*. IEEE, 2014, pp. 4639–4646.

[24] P. A. Bhounsule, "Control of a compass gait walker based on energy regulation using ankle push-off and foot placement," *Robotica*, vol. 33, no. 6, pp. 1314–1324, 2015.

[25] Y. Zhao, B. R. Fernandez, and L. Sentis, "Robust Phase-Space Planning for Agile Legged Locomotion over Various Terrain Topologies." in *Robotics: Science and Systems*, 2016, pp. 557–562.

[26] V. Janardhan and R. P. Kumar, "Online trajectory generation for wide ditch crossing of biped robots using control constraints," *Robotics and Autonomous Systems*, vol. 97, pp. 61–82, 2017.

[27] M. Vukobratovic and D. Juricic, "Contribution to the synthesis of biped gait," *Transactions on Biomedical Engineering*, no. 1, pp. 1–6, 1969.

[28] J. Rebula, F. Canas, J. Pratt, and A. Goswami, "Learning capture points for humanoid push recovery," in *2007 7th IEEE-RAS International Conference on Humanoid Robots*. IEEE, 2007, pp. 65–72.

[29] T. Koolen, T. De Boer, J. Rebula, A. Goswami, and J. Pratt, "Capturability-based analysis and control of legged locomotion, Part 1: Theory and application to three simple gait models," *The international journal of robotics research*, vol. 31, no. 9, pp. 1094–1113, 2012.

[30] M. Krause, J. Englsberger, P.-B. Wieber, and C. Ott, "Stabilization of the capture point dynamics for bipedal walking based on model predictive control," *IFAC Proceedings*, vol. 45, pp. 165–171, 2012.

[31] J. Urata, K. Nshiwaki, Y. Nakanishi, K. Okada, S. Kagami, and M. Inaba, "Online walking pattern generation for push recovery and minimum delay to commanded change of direction and speed," in *2012 IEEE/RSJ International Conference on Intelligent Robots and Systems*. IEEE, 2012, pp. 3411–3416.

[32] M. Shafiee-Ashtiani, A. Yousefi-Koma, M. Shariat-Panahi, and M. Khadiv, "Push recovery of a humanoid robot based on model predictive control and capture point," in *International Conference on Robotics and Mechatronics (ICROM)*. IEEE, 2016, pp. 433–438.

[33] M.-y. Deng, Z.-y. Ma, Y.-n. Wang, H.-s. Wang, Y.-b. Zhao, Q.-x. Wei, W. Yang, and C.-j. Yang, "Fall preventive gait trajectory planning of a lower limb rehabilitation exoskeleton based on capture point theory," *Frontiers of Information Technology & Electronic Engineering*, vol. 20, no. 10, pp. 1322–1330, 2019.

[34] M. Missura, M. Bennewitz, and S. Behnke, "Capture steps: Robust walking for humanoid robots," *International Journal of Humanoid Robotics*, p. 1950032, 2020.

[35] O. E. Ramos and K. Hauser, "Generalizations of the capture point to nonlinear center of mass paths and uneven terrain," in *International Conference on Humanoid Robots*. IEEE, 2015, pp. 851–858.

[36] K. Ochs, "A comprehensive analytical solution of the nonlinear pendulum," *European Journal of Physics*, vol. 32, pp. 479–490, 2011.

[37] M. Olivares and P. Albertos, "Linear control of the flywheel inverted pendulum," *ISA transactions*, vol. 53, no. 5, pp. 1396–1403, 2014.

[38] M. Kasaei, N. Lau, and A. Pereira, "An optimal closed-loop framework to develop stable walking for humanoid robot," in *International Conference on Autonomous Robot Systems and Competitions*. IEEE, 2018, pp. 30–35.